

FIBRE-OPTIC INSTRUMENTS

DOI: 10.1070/QEL16125

Effect of protective coating on random birefringence variations in anisotropic optical fibres in response to temperature changes

S.K. Morshnev, V.P. Gubin, N.I. Starostin, Ya.V. Przhiyalkovsky, A.I. Sazonov

Abstract. **This paper examines for the first time the nature of an anomalous scatter in the birefringence beat length in an anisotropic silica fibre upon changes in its temperature. The effect has been studied by a conventional interferometric technique, using a spectrum analyser. The dispersion of the scatter in the beat length has been shown to be considerably higher at short fibre lengths, which is due to the effect of the protective coating. To interpret the observed effects, a physical model has been proposed which considers random centres, such as microbends, which form and disappear in the protective coating of the fibre in response to temperature changes. The random nature of such local centres may lead to unpredictable changes in the birefringence of anisotropic fibres and, hence, to changes in the sensitivity and accuracy of Faraday effect current sensors.**

Keywords: *optical fibres, birefringence, protective coating.*

1. Introduction

Anisotropic optical fibres include fibres with a high built-in linear birefringence (BR), which are produced by drawing without spinning the preform (PM fibres), and fibres produced by drawing from a spinning preform (spun fibres). All such fibres have a protective coating – typically from urethane acrylates – several tens of microns in thickness. An important issue pertaining to the use of such fibres, e.g. in Faraday effect current sensors [1–3], is stability of their parameters to changes in ambient temperature [2, 4–6]. A key parameter that is measured in experimental studies of such fibres is the beat length L_b of the built-in linear BR, which is usually a linear function of temperature T:

$$L_b = L_{b0}[1 + \alpha(T - T_0)], \tag{1}$$

where L_{b0} is the beat length at temperature T_0 and α is the temperature coefficient, which ranges from 10^{-6} to 10^{-3} K^{-1}, depending on the type of anisotropic fibre and the procedure used to produce artificial built-in BR. The largest coefficient α is offered by fibres containing various stress elements, which differ in thermal expansion coefficients from the fibre material [7]. Microstructured fibres in which built-in BR is due to an elliptical core surrounded by air holes with a refractive index near unity have the smallest temperature coefficient [8, 9].

The beat length of built-in linear BR is often evaluated by analysing interference beat spectra of modes with orthogonal polarisations [10–13]. To this end, the fibre is placed between crossed polarisers. As a result, one obtains not the desired phase BR but group BR [11] in the case of PM fibres or a mixture of phase and group BR in the case of spun fibres [13]. However, the simple measurement procedure and low BR dispersion favour the conventional approach, in which BR dispersion is neglected. The beat length of built-in linear BR is then given by

$$L_b = \frac{\Delta\lambda}{\lambda_0} Z \tag{2}$$

for PM fibre [10] and

$$L_b^2 = \frac{\Delta\lambda}{2\lambda_0} L_{tw} Z \tag{3}$$

for spun fibre [12, 13], where $\Delta\lambda$ is the spectral beat period; λ_0 is the operating wavelength; Z is the length of the fibre section; and L_{tw} is the spin pitch of its helical structure. In our studies, we also used this method.

Fibres fabricated at the V.A. Kotel'nikov Institute of Radio Engineering and Electronics, Russian Academy of Sciences, and by other manufacturers (FiberCore and Nufern) were studied in the temperature range from –60 to +60 °C. For all the fibres, we obtained a linear relation of the form (1) with slightly different temperature coefficients α. We were, however, interested by the large scatter in data (see Fig. 6a). Analysis of standard deviations averaged over the entire temperature range examined indicated that they depended on the fibre segment length Z, whereas calculated parameters L_{b0} and α of the linear relation (1) were independent of fibre length to within the accuracy in our measurements. Stripping the coating caused a drastic decrease in scatter dispersion (see Fig. 6b), which led us to think that the scatter originated from the deformation of the fibre under the effect of the protective coating. The random nature of the scatter in measurement results suggests that temperature changes cause a spontaneous local transformation of polymeric properties in the coating, leading to the formation of random disturbing centres, which appear and disappear in the coating in response to temperature changes in the fibre and influence its BR.

In this paper, we present an experimental and theoretical study of the nature of the anomalous scatter in the measured beat length in an optical fibre with built-in linear BR in

S.K. Morshnev, V.P. Gubin, N.I. Starostin, Ya.V. Przhiyalkovsky, A.I. Sazonov V.A. Kotel'nikov Institute of Radio Engineering and Electronics (Fryazino Branch), Russian Academy of Sciences, pl. Vvedenskogo 1, 141190 Fryazino, Moscow region, Russia; e-mail: nis229@ire216.msk.su

Received 4 May 2016; revision received 20 June 2016
Kvantovaya Elektronika **46** (10) 911–918 (2016)
Translated by O.M. Tsarev

response to temperature changes and interpret the observed effects in terms of a model proposed by us.

2. Theory

2.1. External influences on polarisation fibre

We consider in detail external influences on PM fibre, whose key features persist in the case of external influences on spun fibre. For spun fibre, however, relevant equations cannot be solved in quadratures [14], so no such solutions are presented here.

Let an external influence from some centre induce linear BR, whose major axes lie in a plane normal to the fibre axis and make an angle φ_0 with the respective axes of the built-in linear BR of the PM fibre. Since such centres appear at random, the angle φ_0 is also random. Built-in and induced linear BRs add vectorially, so at a large number of centres the induced linear BRs would be expected to disappear by virtue of averaging over the angle φ_0.

Consider the effect of an individual centre on PM fibre. Let the fibre consist of two segments of length Z_1 and Z_2, both having built-in BR with a phase delay per unit length $\Delta\beta = 2\pi/L_b$, and let induced linear BR, with a phase delay per unit length $\delta = 2\pi/L_{ind}$, act only in segment Z_1, with $Z_1 \ll Z_2$ (L_b and L_{ind} are the beat lengths of the corresponding BRs). The variations in fields E_x and Ey with orthogonal polarisations as the light propagates along the fibre can be represented by a differential matrix, $\| N \|$ (see e.g. Ref. [14]):

$$\left\| \begin{matrix} \frac{dE_x}{dZ} \\ \frac{dE_y}{dZ} \end{matrix} \right\| = \left\| \begin{matrix} i\frac{A}{2} & i\frac{\delta \sin 2\varphi_0}{2} \\ i\frac{\delta \sin 2\varphi_0}{2} & -i\frac{A}{2} \end{matrix} \right\| \left\| \begin{matrix} E_x \\ E_y \end{matrix} \right\|, \quad (4)$$

where $A = \Delta\beta + \delta \cos 2\varphi_0$. Integrating the differential matrix [15], we obtain a Jones matrix, $\| T_1(Z_1) \|$, in segment Z_1:

$$\left\| \begin{matrix} E_x(Z_1) \\ E_y(Z_1) \end{matrix} \right\| = \frac{1}{\Omega} \times \left\| \begin{matrix} \Omega \cos\frac{\Omega Z_1}{2} + iA \sin\frac{\Omega Z_1}{2} & i\delta \sin 2\varphi_0 \sin\frac{\Omega Z_1}{2} \\ i\delta \sin 2\varphi_0 \sin\frac{\Omega Z_1}{2} & \Omega \cos\frac{\Omega Z_1}{2} - iA \sin\frac{\Omega Z_1}{2} \end{matrix} \right\| \left\| \begin{matrix} E_x(0) \\ E_y(0) \end{matrix} \right\|, \quad (5)$$

where $\Omega = \sqrt{\delta^2 \sin^2 2\varphi_0 + A^2}$. It follows from (5) that not only does the induced BR (at $\varphi_0 \neq 0 + m\pi$) change the built-in linear BR, but it also leads to the intermixing of orthogonal modes due to off-diagonal matrix elements [15]. In the absence of induced BR ($\delta = 0$) in segment Z_2, the Jones matrix $\| T_2(Z_2) \|$ reduces to the form

$$\left\| \begin{matrix} E_x(Z_2) \\ E_y(Z_2) \end{matrix} \right\| = \frac{1}{\Delta\beta} \times \left\| \begin{matrix} \Delta\beta \cos\frac{\Delta\beta Z_2}{2} + i\Delta\beta \sin\frac{\Delta\beta Z_2}{2} & 0 \\ 0 & \Delta\beta \cos\frac{\Delta\beta Z_2}{2} - i\Delta\beta \sin\frac{\Delta\beta Z_2}{2} \end{matrix} \right\| \times \left\| \begin{matrix} E_x(0) \\ E_y(0) \end{matrix} \right\|. \quad (6)$$

If light passes first through segment Z_1 and then through segment Z_2, the fields of the orthogonal modes can be calculated using the matrix product

$$\left\| \begin{matrix} E_x(Z_1 + Z_2) \\ E_y(Z_1 + Z_2) \end{matrix} \right\| = \| T_2(Z_2) \| \| T_1(Z_1) \| \left\| \begin{matrix} E_x(0) \\ E_y(0) \end{matrix} \right\|. \quad (7)$$

In experiments, a fibre to be studied is placed between crossed polarisers so that the major axes of its built-in BR are at 45° to the transmission plane of the polarisers. In this simplest scheme, the output intensity is

$$I = [E_x(Z_1 + Z_2) + E_y(Z_1 + Z_2)][E_x^*(Z_1 + Z_2) + E_y^*(Z_1 + Z_2)]/2 = I_0\left[1 + \frac{\delta^2 \sin^2 2\varphi_0}{\Omega^2} \cos(\Delta\beta Z_2) + \frac{A^2}{\Omega^2} \cos(\Delta\beta Z_2)\cos(\Omega Z_1) - \frac{A}{\Omega} \sin(\Delta\beta Z_2)\sin(\Omega Z_1)\right]. \quad (8)$$

In passing to the wavelength dependence, we take into account the following:

1. BR dispersion can be neglected near the operating wavelength, i.e. we take $n_x - n_y \approx$ const.

2. The wavelength dependence of $\Delta\beta$ takes the form $\Delta\beta = (\lambda_0/\lambda)(2\pi/L_{b0})$, where L_{b0} is the beat length of the built-in BR at the operating wavelength λ_0.

3. There is an analogous dependence for the linear BR induced by an external influence: $\delta = (\lambda_0/\lambda)(2\pi/L_{ind0})$.

4. The spatial frequency can be represented in the form

$$\Omega = \frac{\lambda_0}{\lambda}\Omega_0 = \frac{\lambda_0}{\lambda}\left[\left(\frac{2\pi}{L_{b0}} + \frac{2\pi}{L_{ind0}} \cos 2\varphi_0\right)^2 + \left(\frac{2\pi}{L_{ind0}} \sin 2\varphi_0\right)^2\right]^{1/2}. \quad (9)$$

5. We call attention to the fact that the coefficients of the sines and cosines in (9) are independent of wavelength λ.

It is the wavelength dependence of intensity (8) that is observed on the display of a spectrum analyser in experiments. In the absence of external influences, we have $\delta = 0$ and therefore $\Omega = \Delta\beta$. Relation (8) then takes the form

$$I = I_0[1 + \cos\Delta\beta(Z_1 + Z_2)]. \quad (10)$$

To more accurately determine polarisation beat minima, let us present function (8) in a semilog plot, analogous to what is seen on the display of a spectrum analyser. For the same reason, the wavelength step is chosen to be 0.02 nm. Figure 1 shows beat spectra for different $2\varphi_0$ angles (doubled φ_0 corresponds to representation on the Poincare sphere). It follows from Fig. 1 that, depending on the angle $2\varphi_0$, the visibility of the interference pattern may decrease (with the lowest visibility at $2\varphi_0 = 45°$ and 135°), which will lead to an increased error in the determination of the wavelength difference $\Delta\lambda$ between two neighbouring minima, necessary for calculating the beat length of built-in BR by formula (2). Such a decrease in fringe visibility is indeed observed in experiments. Relation (8) has three spatial dependences, on $\Delta\beta Z_2$, $\Delta\beta Z_2 - \Omega Z_1$ и $\Delta\beta Z_2 + \Omega Z_1$, which may result in 'visibility resonances' in the beat spectrum. For example, at $L_{b0} = 9$ mm, $L_{ind0} = 0.1$ mm, $Z_2 = 2$ m and $Z_1 = 0.347$ mm, the beat visibility near the operating wavelength $\lambda_0 = 1550$ nm is nearly zero.

Figure 2 shows a 'correction' ΔL_b due to an external influence with a beat length L_{ind}, acting over a length Z_1, to the beat length L_b, determined over a length Z_2, as a function of angle $2\varphi_0$. Where possible, we avoided visibility resonances.

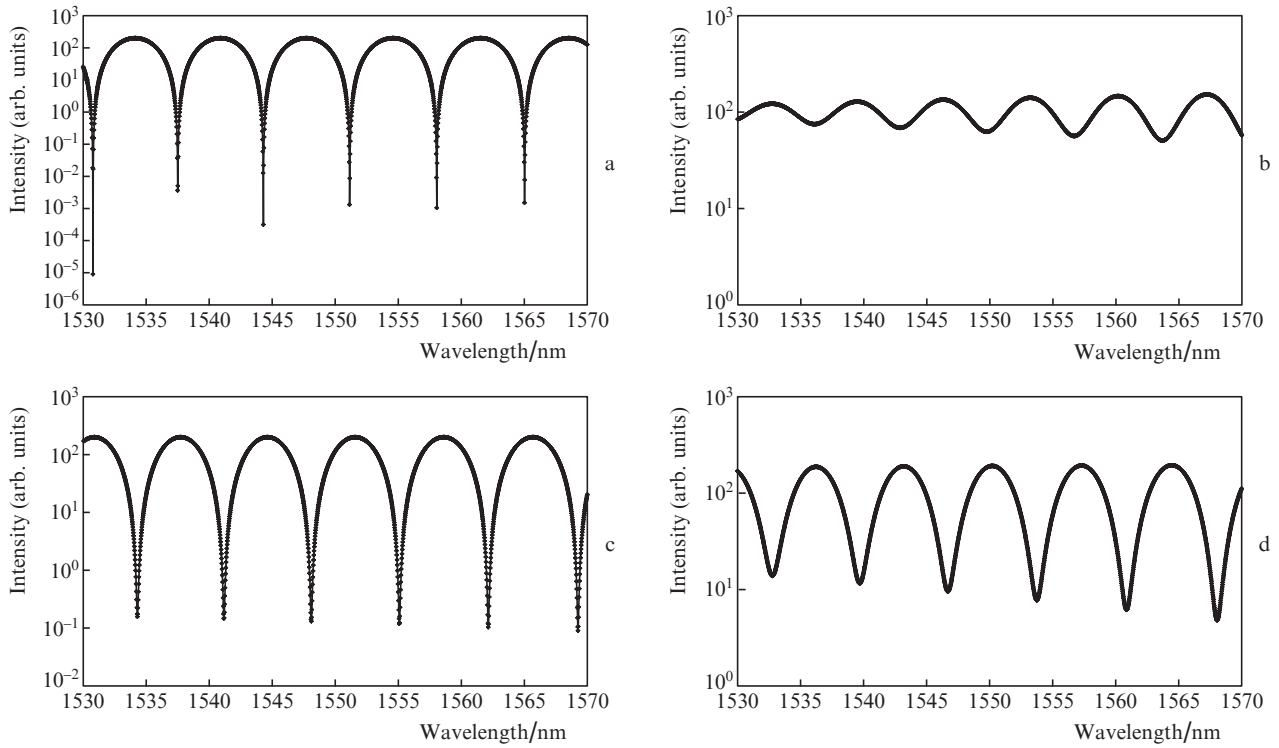

Figure 1. Calculated polarisation beat spectra for built-in and induced BR in PM fibre at $L_{b0} = 9$ mm, $L_{ind0} = 0.3$ mm, $Z_1 = 1$ mm, $Z_2 = 2$ m and $2\varphi_0 =$ (a) 0, (b) 45°, (c) 90° and (d) 150°.

Note that the change in L_b reaches several percent. At $2\varphi_0 \approx 90°$, the additional contribution to L_b is zero. Moreover, this contribution changes sign at $2\varphi_0 = 90°$. Thus, the contributions of centres at $2\varphi_0 < 90°$ can be compensated for by those at $2\varphi_0 > 90°$.

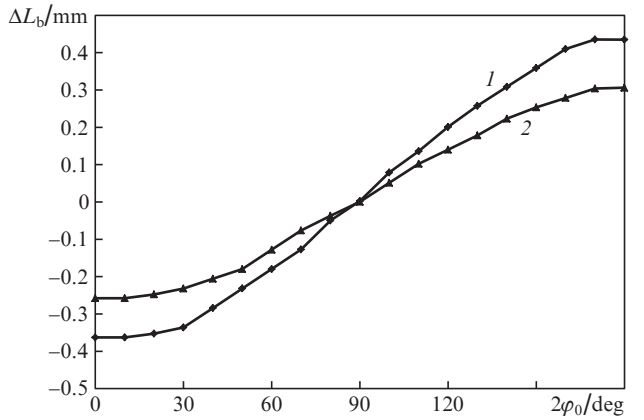

Figure 2. Calculated microbend contribution ΔL_b to the beat length L_b as a function of angle $2\varphi_0$ at $L_{b0} = 9$ mm, $L_{ind0} = 0.1$ mm, $Z_2 = 2$ m and $Z_1 =$ (*1*) 1 and (*2*) 0.694 mm.

In the case represented in Fig. 3, a fibre bend was chosen as an external influence. It is seen that increasing the fibre length Z_1 over which it acts or the local influence itself (reducing L_{ind0}) leads to an increase in the contribution $|\Delta L_b|$ to the net L_b. At a beat length $L_{ind0} = 1$ mm, the contribution to L_b exceeds 0.1 mm even at $Z_1 = 4$ mm.

Thus, strong external influences (exceeding built-in ones) acting on short lengths of fibre and separated by considerably longer sections ($Z_2 = 2$ m) may make appreciable contributions to the measured net beat length L_b of built-in BR. Their contributions at $2\varphi_0 < 90°$ can be compensated for by those at $2\varphi_0 > 90°$.

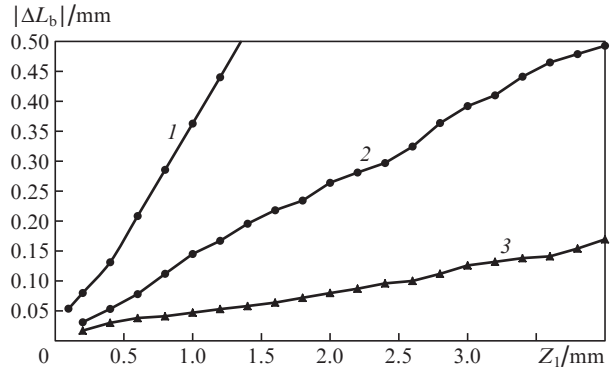

Figure 3. Calculated contribution $|\Delta L_b|$ to the beat length as a function of bend (external influence) length Z_1 for a PM fibre of total length $Z_1 + Z_2$ ($Z_2 = 2$ m) at induced beat lengths $L_{ind0} =$ (*1*) 0.1, (*2*) 0.3 and (*3*) 1.0 mm.

2.2. Random centres. Poisson distribution

We are interested in the probability that a fibre segment of length x contains r centres capable of changing the average BR of the segment. The following assumptions are thought to be true:

1. The formation of a centre in a fibre segment of length x is independent of whether such centres were present there before.

2. The probability that a centre is present in a short segment of length δx is proportional to this length. In other words, the probability that a centre is present in a segment from x to $x + \delta x$ is $\eta\delta x + o(\delta x)$, where $o(\delta x)$ has a higher order of smallness than does δx.

3. The probability that two or more centres are present in a given fibre segment is $0 + o(\delta x)$, i.e. zero.

It is easy to see (see e.g. Hudson [16]) that these assumptions lead us to the Poisson distribution. If the probability that an event occurs in an interval (of space, time etc.) Δx is $\eta\delta x$, where η is a constant, the probability P that, in a final interval of length x, the event will occur independently k times follows the Poisson distribution [16]

$$P(k) = \frac{K^k}{k!}\exp(-K), \tag{11}$$

where $K = \eta x$ is the mean number of events in an interval of length x. The mean number of events is K and the standard deviation is $\sqrt{K}$. An estimate of the parameter η is k/x, with a standard deviation $\sqrt{k/x}$. The Poisson probability distribution allows one to calculate probabilities of rare events.

Let Δx be the length of a fibre segment containing on average one centre, i.e. $\eta\Delta x = 1$. Let us determine the probability that N centres are present in a segment of length $x = N\Delta x$; $k = x/\Delta x = N$. From (11), we obtain

$$P(N) = \frac{(\eta N\Delta x)^N}{N!}\exp(-\eta N\Delta x) = \frac{N^N(1)^N}{N!\exp N}. \tag{12}$$

The factorial in the denominator of (12) can be expressed through the gamma function (Sonin's formula) [16]:

$$N! = \Gamma(1 + N) \approx \sqrt{2\pi}\,N^{N+1/2}\exp\left(-N + \frac{1}{12N}\right). \tag{13}$$

This formula can also be used in the case of half-integer N values. Substituting (13) into (12), we obtain

$$P(N) = \frac{1}{\sqrt{2\pi N}}\exp\left(-\frac{1}{12N}\right). \tag{14}$$

Thus, at a long length of fibre, the probability of the presence of N centres is inversely proportional to the square root of the fibre length.

The probability that one more centre ($k = N + 1$) appears in a segment of length x containing on average $K = N$ centres is

$$P(K = N, k = N + 1) = \frac{N^{N+1}}{(N + 1)!\exp N}. \tag{15}$$

Substituting (13) for the factorial, we obtain

$$P(K = N, k = N + 1) = \left(\frac{N}{N + 1}\right)^{N+1}\frac{1}{\sqrt{2\pi(N + 1)}} \times \exp\left[1 - \frac{1}{12(N + 1)}\right]. \tag{16}$$

The formation of an additional centre with probability (16) at a mean number of centres $K = N$ can be realised in our experiments at a long length of fibre.

At a short length of fibre, we can take that $N = x/\Delta x$, as above, but the segment length Δx corresponding on average to one centre here exceeds the length of the fibre segment under consideration: $\Delta x > x$, i.e. $N < 1$. Let us find the probability that a single centre is present in a segment of length x. The mean number of centres is $K = \eta x = \eta N\Delta x = N$ ($k = 1$). Relation (11) takes the form

$$P(1) = N\exp(-N). \tag{17}$$

At low N values ($N < 1$), the probability $P(1)$ scales linearly with N and, hence, with the fibre length x. Similarly, at a mean number of centres $K = N$, the probability that there are two centres ($k = 2$) is

$$P(2) = (N^2/2)\exp(-N), \tag{18}$$

and the probability of three centres ($k = 3$) is

$$P(3) = (N^3/6)\exp(-N). \tag{19}$$

With increasing fibre length, the measurement error changes from (17) to (16), with a maximum at $N \approx 1$. For $N < 1$ ($\Delta x > x$), increasing the fibre length leads to an increase in the observed standard deviation of the beat length L_b in proportion to the fibre length. At long lengths of fibre ($N \gg 1$, $\Delta x \ll x$), increasing the fibre length reduces the standard deviation in accordance with (16). Moreover, the effects of centres compensate for each other (the mean effect is zero because of the averaging over the azimuth).

3. Experimental

3.1. Experimental setup and data processing techniques

Figure 4 shows a schematic of the experimental setup. As a broadband light source (*1*), we used an ESS-30-M-01 superluminescent erbium-doped fibre oscillator, which allowed light of 5–7 mW power with a –60 dBm bandwidth of about 90 nm and wavelength near $\lambda = 1550$ nm to be coupled into single-mode fibre. The light from the source (*1*) was directed to a fibre-optic polariser (*2*) with an extinction of at least 35 dB throughout the band. The linearly polarised light passed through a fusion splice (*3*) and entered the fibre under study (*4*), enclosed in a thermal chamber (*5*). Next, after passing through another fusion splice (*6*) and a fibre-optic analyser (*7*) similar to the polariser (*2*), the light was fed to a Yokogawa AQ6370C spectrum analyser at the minimum adjustable spectral resolution $\gamma_1 = 0.017$ nm. The fusion splices (*3*, *6*) were made so that the polarisation axes of the two fibres made an

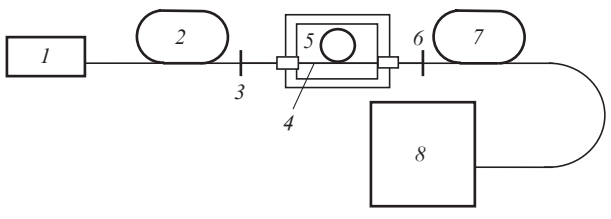

Figure 4. Schematic of the experimental setup:
(*1*) broadband optical source; (*2*) fibre-optic polariser; (*3*, *6*) fusion splices; (*4*) fibre under investigation; (*5*) thermal chamber; (*7*) fibre-optic analyser; (*8*) spectrum analyser.

angle of 45°. The thermal chamber (*5*) allowed the temperature to be controlled and maintained with an accuracy of ±0.2° in the range from –60 to +60 °C.

Figure 5 shows a typical experimental spectrum as observed on the display of the spectrum analyser. We see an interference spectrum on a semilog scale, superimposed over the emission spectrum of the superluminescent erbium-doped fibre source (*1*). The boxes in the bottom part of the screen indicate the boundary and centre wavelengths of the range under investigation (1530, 1560 and 1590 nm, respectively) and the division value on the horizontal axis of the screen (6 nm div^{-1}). Displayed in the top part of the screen are the division value on the vertical axis of the screen (10 dB div^{-1}), the spectral resolution along the horizontal axis (RES, 0.02 nm), the averaging time (AVG, 1 s) and the number of data points in the sample (SMPL, 15 001). Settings specify a spectral resolution of 0.017 nm, and the 0.02-nm resolution indicated on the screen seems to be a rounded value.

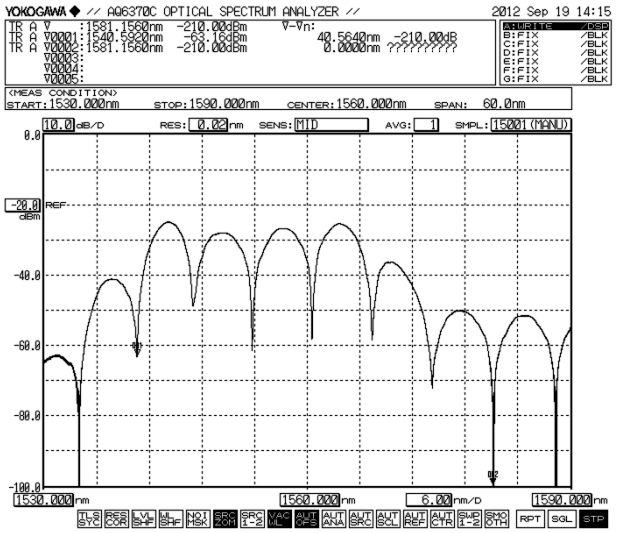

Figure 5. Typical experimental polarisation beat spectrum as observed on the display of a spectrum analyser.

In our measurements, the spectral resolution γ_1 of the spectrum analyser is also instrumental uncertainty $\gamma_1(\lambda)$ in the wavelength measured by this instrument, which determines its relative accuracy. Samples (data points of the spectrum) are 0.004 nm apart and might ensure a better spectral resolution. The marker that is used to measure wavelengths moves across the spectrum with a step of 0.002 nm. Note that the calculated interference beat spectrum presented in Fig. 1c is very similar to the experimental spectrum in Fig. 5.

The beat length was measured as follows: First we measured the wavelength difference $\Delta\lambda$ between two minima in the spectrum at wavelengths λ_1 and λ_2 in the vicinity of the operating wavelength (1550 nm). Next, we calculated the beat length L_b^{ex} by formulas (2) and (3) for PM and spun fibres, respectively. The wavelength λ_0 in these formulas was taken to be the average

$$\lambda_0 = (\lambda_1 + \lambda_2)/2. \tag{20}$$

In the thermal chamber, fibre was either placed as a free coil (in the case of short pieces) or inserted into a thin quartz tube bent to a 20-cm-diameter ring. The temperature in the thermal chamber was varied at a rate of 40 °C h^{-1}. The measurements were performed either during constant variations in temperature or at fixed temperatures for 10–15 min per data point. No drastic differences were detected between the results obtained by these two procedures. The temperature was scanned first in one direction (for example, from +60 to –60 °C) and then always in the opposite direction. No hysteresis was detected.

The measured beat length $L_b^{ex}(T_i)$ was presented in a figure together with a graph of function (1), which had the form of a straight line. The number of data points ($i = 1, ..., M$) was $M = 25–50$. The parameters L_{b0} and α in the linear relation were extracted from experimental data by least squares fitting. For each data point, we calculated the square of the deviation from function (1), $L_b(T_i)$, at the same temperature: $[L_b^{ex}(T_i) - L_b(T_i)]^2$. All the squares of the deviations were added up. Varying the parameters L_{b0} and α, we minimised the sum of the squares of the deviations. From this sum, we obtained the standard deviation γ_{ex} for an individual beat length L_b measurement,

$$\gamma_{ex} = \left\{[1/(M-1)]\sum_{i=1}^{M}[L_b^{ex}(T_i) - L_b(T_i)]^2\right\}^{1/2} \tag{21}$$

(since the number of data points is comparatively small, the average is taken over $M - 1$ data points) and relative uncertainty of the measurement:

$$\sigma_{ex} = \gamma_{ex}/L_{b0}. \tag{22}$$

The indicated relative uncertainties as functions of fibre length for various fibres were represented in a figure.

Relative measurement error σ_{ex} is contributed by instrumental error, $\sigma_{ap} = \gamma_1(\Delta\lambda)/\Delta\lambda$, and the relative error σ_{in} due to an external perturbation centre:

$$\sigma_{ex}^2 = \sigma_{in}^2 + \sigma_{ap}^2. \tag{23}$$

Therefore, the latter relative error can be found as

$$\sigma_{in} = \sqrt{\sigma_{ex}^2 - \sigma_{ap}^2}. \tag{24}$$

3.2. Experimental results

Figure 6 illustrates the effect of the protective coating of fibre on the scatter in the beat length as a function of temperature. In a 2.5-m length of a PM silica fibre with a temperature-compensated cladding, the beat length L_b was a relatively weak function of temperature ($\alpha \approx 2\times10^{-4}$ K^{-1}), but the measurement results showed a large scatter (Fig. 6a). Using least squares fitting, we obtained a straight line with parameters $L_{b0} = 4.413 \pm 0.042$ mm and $\alpha = 2.5\times10^{-4}$ K^{-1}. Relative error was determined to be $\sigma_{ex} = 0.0096$, whereas the relative instrumental error of the spectrum analyser, evaluated from manufacturer data, was $\sigma_{ap} = 0.0056$.

After the measurements, the fibre was stripped of its coating and the measurements were repeated using a 2.25-m length of the fibre. The results are presented in Fig. 6b. We obtained $L_{b0} = 4.397 \pm 0.011$ mm and $\alpha = 2.05\times10^{-4}$ K^{-1}, with a sharp decrease in scatter. Relative error, $\sigma_{ex} = 0.0024$, is a factor of 4 smaller than that in the case of the coated fibre, and is even smaller than $\sigma_{ap} = 0.0056$. This finding led us to assume that the true spectral resolution $\gamma_1(\Delta\lambda)$ of the spectrum

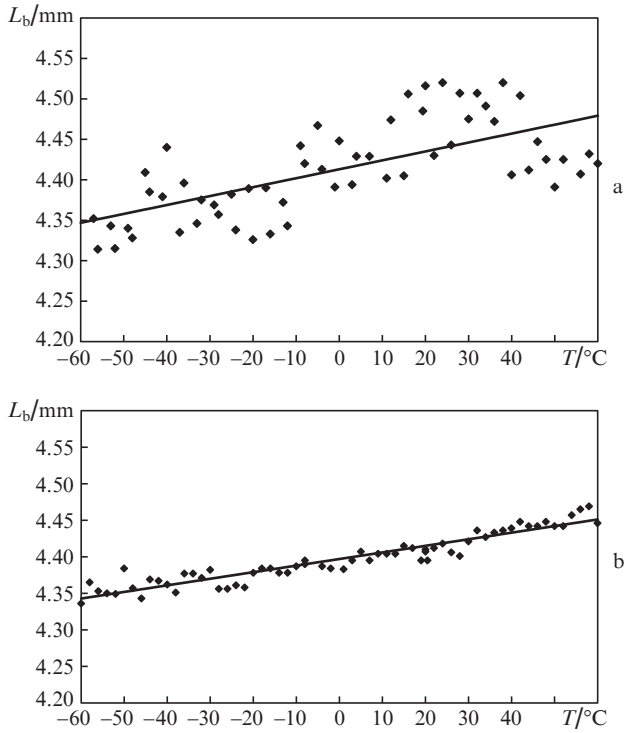

Figure 6. Temperature dependences of the experimentally determined beat length of linear BR in (a) a $Z = 2.5$ m length of a coated PM fibre and (b) a $Z = 2.25$ m length of stripped fibre.

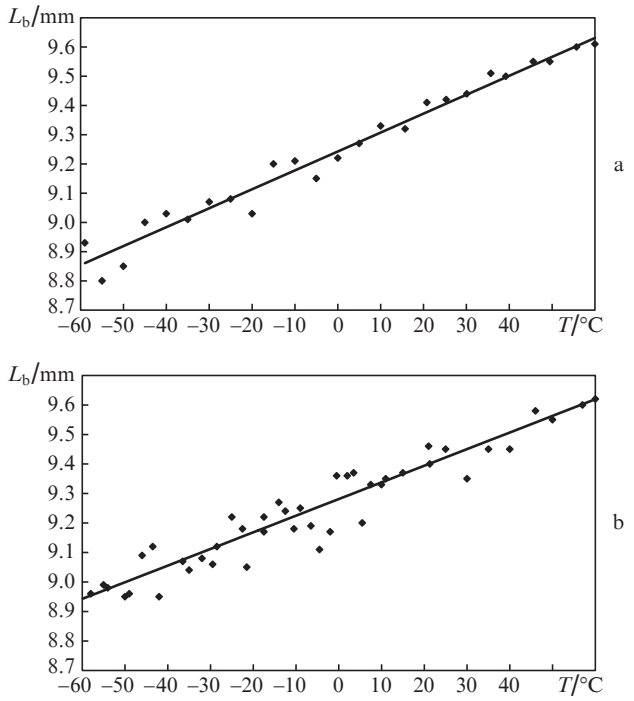

Figure 7. Temperature dependences of experimentally determined beat lengths L_b for two spun fibres: (a) $Z = 20$ m, $L_{b0} = 9.24 \pm 0.04$ mm, $\alpha = 7\times10^{-4}$ K^{-1}, $\sigma_{ex} = 0.0043$, $\sigma_{ap} = 0.0017$, $\Delta\lambda = 4.414$ nm; (b) $Z = 4$ m, $L_{b0} = 9.28 \pm 0.06$ mm, $\alpha = 6.8\times10^{-4}$ K^{-1}, $\sigma_{ex} = 0.0062$, $\sigma_{ap} = 0.0003$, $\Delta\lambda = 22.248$ nm.

analyser was even better than that specified by its manufacturer. Indeed, the relative instrumental error σ'_{ap} can also be estimated from above in a similar way [see Eqn (23)] from experimental error for stripped fibre, which has $\sigma_{in} = 0$. Relative error $\sigma_{ex} \approx \sigma'_{ap}$ in this experiment is 0.0024. At a difference $\Delta\lambda = \lambda_1 - \lambda_2 = 3.03$ nm, this corresponds to uncertainty in wavelength (or spectral resolution) $\gamma_1(\Delta\lambda) = 0.0073$ nm. Subsequently, we used the estimated error in the wavelength difference between neighbouring spectral minima in calculating relative error σ_{ap} for other experimentally determined $\Delta\lambda$ and σ_{in} values by Eqn (24).

From the data presented in Fig. 6a, we can also determine the random relative error σ_{in} due to the protective coating of the fibre:

$$\sigma_{in} = \sqrt{\sigma_{ex}^2 - \sigma_{ap}'^2} = \sqrt{(0.0096)^2 - (0.0024)^2} = 0.0093.$$

Figure 7 illustrates the above data processing techniques. It shows temperature dependences of experimentally determined beat lengths for two different lengths ($Z = 20$ and 4 m) of spun fibre. Comparison of Figs 7a and 7b indicates that reducing the fibre length Z leads to an increase in the scatter of the data about a straight line of the form (1) with parameters L_{b0} and α determined by least squares fitting.

The experimental relative errors σ_{ex} were determined by formulas (21) and (22) for a large number of fibre samples differing in both length Z and L_{b0}.

Figure 8 shows relative error σ_{ex} as a function of fibre length Z for all the samples studied. We investigated three types of PM fibre, differing in beat length L_{b0}, and spun fibres similar in beat length ($L_{b0} \approx 9$ mm). Using the experimentally determined instrumental error $\gamma_1(\Delta\lambda) = 0.0073$ nm in $\Delta\lambda$ measurements, we evaluated relative instrumental error as a function of Z for these four types of fibre (Fig. 8, straight lines).

In Fig. 8, random variations in beat lengths are seen to increase with decreasing fibre length in the range $Z \approx 1-3$ m and to gradually decrease in proportion to $\sqrt{Z}$ with increasing fibre length in the range $Z \approx 7-20$ m (approaching instrumental error).

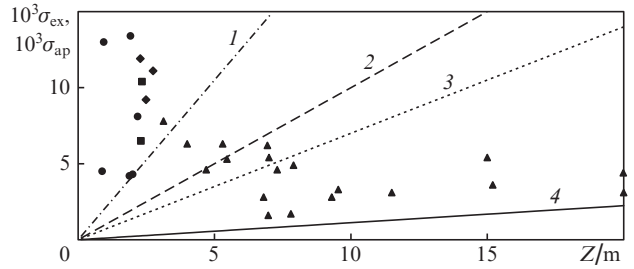

Figure 8. Experimentally determined relative error σ_{ex} in beat length (L_b) measurements (data points) and relative instrumental error (lines) as functions of sample length Z for PM fibre with $L_{b0} = 2.3$ (◆, *1*), 4.8 (■, *2*) and 6.8 (●, *3*) mm and spun fibre with $L_{b0} = 9$ mm (▲, *4*).

4. Discussion

One important parameter in measurements of the beat length in anisotropic fibres is the length of the fibre segment Z. According to (2) and (3), the measured interference beat interval $\Delta\lambda$ is inversely proportional to Z. With decreasing fibre length, $\Delta\lambda$ increases and relative measurement error σ_{ap} decreases. This would be expected to lead to a reduction in relative error σ_{ex}. However, reducing the fibre length Z upon changes in temperature, we encountered an increase in σ_{ex}. We assume that the main cause of this effect is the formation

of perturbation centres in the fibre coating, which induce additional linear BRs whose axes are oriented at random with respect to the built-in BR axes. The estimates in Section 2.1 indicate that the induced BRs should be sufficiently high ($L_b < 1$ mm) if they act in short pieces of fibre.

The random azimuthal orientation of perturbation centres at a sufficiently large number of such centres leads to mutual compensation of their effects. Because of this, their influence decreases with increasing fibre length. The assumptions presented in Section 2.2 lead us to conclude that the centres follow the Poisson distribution. At a large number of centres, the probability of their formation is inversely proportional to the square root of the average number of centres, i.e. inversely proportional to the square root of the fibre length Z. At the same time, at fibre lengths with average $N \approx 1-3$, deviations from this relationship are possible. Indeed, the Poisson distribution (11) allows one to calculate the probability of the formation of just one centre (or two centres) in a segment with a mean number of centres e.g. $N = 3$. These probabilities approach that of the formation of three centres and hence can be realised in experiments.

Figure 9 shows relative induced error σ_{in} calculated by formula (24), i.e. relative error without instrumental error. In addition, the solid lines in Fig. 9 represent functions proportional to the probabilities of the formation of just one new centre [see Eqn (17)], two centres [see Eqn (18)], three centres [see Eqn (19)] and $N + 1$ centres [see Eqn (16)] in a segment of length Z at a mean number of centres N. The mean number of centres N can be calculated as

$$N = Z/\Delta x, \tag{25}$$

where Δx is the length over which on average one centre appears. For dependences proportional to probabilities, Δx is adjusted as a parameter.

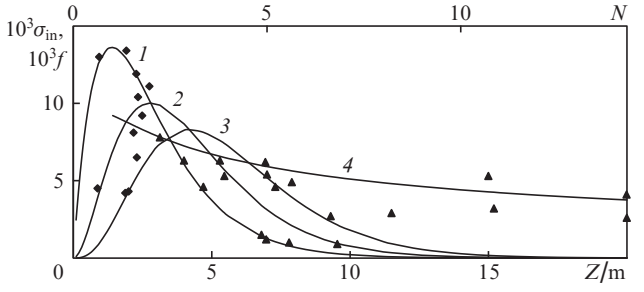

Figure 9. Experimentally determined relative error σ_{in} (data points) in measurements of the length of beats induced by the protective coating vs. fibre length Z for spun fibre (▲) and PM fibre (◆). The solid lines represent functions $f = 0.037P$ proportional to the probabilities of the formation of (*1*) just one centre, (*2*) two centres, (*3*) three centres and (*4*) $N + 1$ centres in the coating at a mean number of centres N.

For all the dependences presented in Fig. 9, we chose the same value $\Delta x = 1.4$ m and a single proportionality coefficient 0.037 between probabilities of the formation of centres and relative errors σ_{in}. A change in Δx by 0.05 m or in the proportionality coefficient by 0.005 leads to a dramatic discrepancy (by several times) between theoretical and experimental data. It is seen from Fig. 9 that the minimum and maximum values of σ_{in} are well represented by curves (*1*) and (*4*), and the other experimentally determined σ_{in} values can be accounted for with allowance for the probabilities of the formation of several centres in a number less than the average number N. It should be emphasised that we deal with relative errors in BR measurements due to random events, so the degree of uncertainty in measurements is proportional to $1/\sqrt{N}$ and, hence, increases sharply for $N \to 1$. The above estimates do not take into account that the magnitude of an effect depends on its azimuthal orientation. For example, in Fig. 9 three data points with low σ_{in} values ($\sim$0.001) may be related to the orientation near $2\varphi_0 \approx 90°$ (see Fig. 2) or the simultaneous formation of two centres that have opposite effects and compensate for each other.

The most likely cause of changes in linear BR in anisotropic fibres is bends. The major axes of bend-induced linear BR lie in the plane of the bend along its radius and along the normal to this plane. The axes intersect on the fibre axis. One possible cause of bending is the thermal expansion mismatch between the silica fibre and protective coating. The effect of coating-induced bends on the loss in fibres was investigated by Yeung and Johnston [17]. The effect can be aggravated by axial misalignment of the coating and fibre or inhomogeneity of the coating, in particular by the formation of crystals in the coating material [18]. It is worth noting that minimum relative errors were obtained at room temperature, without scanning the temperature. It seems likely that any temperature changes are favourable for the formation of centres responsible for additional BR. At low temperatures (from about –50 to –60 °C), we often observe significant differences in length between two neighbouring beats, which can be interpreted as evidence that a centre can form or disappear even during scanning between two minima at λ_1 and λ_2 (10–20 s).

The formation of local centres capable of inducing additional BR upon temperature changes may lead to unpredictable changes in the sensitivity of Faraday effect sensors despite the monotonic, linear variation of the beat length with temperature, especially in the case of short pieces of magnetically sensitive spun fibre.

5. Conclusions

We have studied the nature of an anomalous scatter in the beat length in an optical fibre with built-in linear BR upon temperature changes and proposed a physical model for random centres that explains effects observed in experiments.

A slow, monotonic variation in the temperature of anisotropic silica fibres has been shown to be accompanied by random variations in BR, detected in measurements of the polarisation beat length by a conventional technique, using a spectrum analyser. The magnitude of the variations in BR depends on the fibre length, reaching several percent at a small fibre length and dropping to zero at a long length. When a constant temperature is reached, the BR of the fibre returns to its original level, i.e. variations do not accumulate. We have demonstrated that no such variations occur in stripped fibre. One possible cause of the observed effect is the formation of random local centres in the protective coating of the fibre, such as temperature-induced microbends, which influence the parameters of the fibre. Local effects may compensate each other, so the net effect decreases with increasing fibre length. The effects in question produce significant changes in the built-in BR of the fibre, which, in particular, influences the magneto-optical sensitivity of spun fibres that are used as sensing elements in Faraday effect fibre-optic current sensors. The random nature of the observed effects may lead to unpre-

dictable changes in the sensitivity and accuracy of such current sensors.

References

1. Enokihara A., Isutsu M., Sueta T. *J. Lightwave Tehnol.*, **5**, 1584 (1987).
2. Laming R.I., Payne D.N. *J. Lightwave Technol.*, **7** (12), 2084 (1989).
3. Bohner K., Gabus P., Nehring J., Brandle H. *J. Lightwave Tehnol.*, **20**, 267 (2002).
4. Gubin V.P., Isaev V.A., Morshnev S.K., et al. *Kvantovaya Elektron.*, **36** (3), 287 (2006) [*Quantum Electron.*, **36** (3), 287 (2006)].
5. Bassett M., Bjarm M., Chan D., et al. *Proc. SPIE Int. Soc. Opt. Eng.*, **3860**, 501 (1999).
6. Mohr F., Schadt F. *Proc. SPIE Int. Soc. Opt. Eng.*, **5502**, 410 (2004).
7. Zhang F., Lit J.W.Y. *Appl. Opt.*, **32** (13), 2213 (1993).
8. Michie A., Canning J., Lyytikainen K., et al. *Opt. Express*, **12** (21), 5160 (2004).
9. Chamorovsky Yu.K., Starostin N.I., Ryabko M.V., et al. *Proc. Int. Conf. on Materials for Advanced Technologies (ICMAT-2009)* (Singapore, 2009) pp 110–112.
10. Kikuchi K., Okoshi T. *Opt. Lett.*, **8**, 122 (1983).
11. Rashleigh S.C. *Opt. Lett.*, **8**, 336 (1983).
12. Morshnev S.K., Ryabko M.V., Chamorovskii Y.K. *Proc. SPIE Int. Soc. Opt. Eng.*, **6594**, 6594OR (2007).
13. Morshnev S.K., Gubin V.P., Przhiyalkovsky Ya.V., Starostin N.I. *Kvantovaya Elektron.*, **43** (12), 1143 (2013) [*Quantum Electron.*, **43** (12), 1143 (2013)].
14. Azzam R.M.A., Bashara N.M. *Ellipsometry and Polarized Light* (Amsterdam: North-Holland, 1977; Moscow: Mir, 1981).
15. Ulrich R., Rashleigh S.C. *IEEE J. Quantum Electron.*, **QE-18** (12), 2032 (1982).
16. Hudson D.J. *Lectures on Elementary Statistics and Probability* (Geneva: CERN, 1963; Moscow: Mir, 1970).
17. Yeung W.F., Johnston A.R. *Appl. Opt.*, **17**, 3703 (1978).
18. Wunderlich B. *Macromolecular Physics, Vol. 2: Crystal Nucleation, Growth, Annealing* (New York: Academic, 1976; Moscow: Mir, 1979).